processes

MDPI

Article

Static Characteristics of Friction Block Teeth of Coiled Tubing Drilling Robot

Shuo Han [1], Xiaohua Xiao [1], Jianguo Zhao [1,2,*], Xin Zhao [1] and Ruifan Yang [3,4]

[1] School of Mechatronic Engineering, Southwest Petroleum University, Chengdu 610500, China
[2] State Key Laboratory of Oil and Gas Reservoir Geology and Exploitation, Chengdu, University of Technology, Chengdu 610059, China
[3] School of Mechatronic Engineering, Xi'an Shiyou University, Xi'an 710065, China
[4] China Petroleum Group Chuanqing Exploratory Drilling Engineering Co., Ltd., Drilling Exploiting Engineering Technology Research Institute, Deyang 618300, China
* Correspondence: 202099010015@swpu.edu.cn

Abstract: Conventional downhole traction robots only provide axial traction, while coiled tubing drilling (CTD) robots must not only overcome the axial force but also overcome the reaction torque generated by the drill bit breaking the rock. Therefore, the tooth profile of the friction block of the conventional downhole traction robot cannot achieve effective support under the simultaneous action of the axial load and circumferential load. In this paper, based on the actual reaction torque conditions generated by CTD, a mechanical model of the friction block teeth of the CTD robot under the conditions of axial traction and reverse torque is established. This reveals the influence of different tooth slope angles, axial-included angles and friction coefficients on the mechanical properties. It provides guidelines for the design of the inclination of the tooth slope, the axial angle of the tooth and the friction coefficient of the friction block of the CTD robot. It has scientific and engineering significance for the promotion of downhole robots in drilling engineering.

Keywords: coiled tubing drilling; drilling robot; friction block teeth; static characteristics

Citation: Han, S.; Xiao, X.; Zhao, J.; Zhao, X.; Yang, R. Static Characteristics of Friction Block Teeth of Coiled Tubing Drilling Robot. *Processes* **2023**, *11*, 2201. https://doi.org/10.3390/pr11072201

Academic Editor: Jiangxin Wang

Received: 8 March 2023
Revised: 12 March 2023
Accepted: 20 March 2023
Published: 22 July 2023

1. Introduction

Coiled tubing drilling technology is relatively mature at present, and it has the advantages of a short operation cycle [1], low pollution (small waste treatment volume), and cost saving [2]. When operating in a horizontal well, the coiled tubing cannot enter the well by its own gravity, and the tubing string in the well will be subjected to the axial friction of the well wall, causing problems of buckling and "locking up" [3], making it difficult to run the tubing string [4,5]. Some scholars have used mechanical drag reduction [6] and lubrication [7] to reduce the drag reduction to extend the length of the pipe string, but the total extension length is far from enough. For example, Yue et al. [8] used real drilling data for analysis: under the condition of 10 kN effective WOB, the extension length of the horizontal section is less than 150 m. The difficulty of running the coiled tubing drilling string severely limits the popularization and application of coiled tubing drilling technology in extended reach directional wells and horizontal wells.

In response to the above problems, Hallundaek [9] designed the first underground traction robot in 1987. Formica et al. [10] invented a towing robot with multiple support mechanisms and traction mechanisms. This towing robot has good obstacle clearance performance and can adapt to complex underground environments. In logging operations, the towing robot designed by Duthie et al. [11] can perform real-time data measurement and analysis on small wells over 10,000 feet. At present, downhole tractors are also developing from a simple traction function to a drilling robot with "traction and drilling integration", but there are no reports of field applications.

Research has found that the friction teeth in the supporting mechanism of the drilling robot have a greater impact on its supporting performance. In recent years, some scholars only carried out related mechanical studies on the obstacle crossing performance, nonlinear dynamics, sealing performance, control performance and frictional resistance of drilling robots [12–16]. Further research on the support mechanism only stays in the optimization design of the support mechanism [17,18]. At present, the research on the mechanical characteristics of downhole drilling robots mainly focuses on the mechanical characteristics of its supporting mechanism, and there is no research on the mechanical characteristics of the friction block teeth of the drilling robot.

In this paper, based on the actual reaction torque conditions generated by coiled tubing drilling, a static model of the friction block teeth of the coiled tubing drilling robot under the conditions of axial traction and reverse torque is established, and the friction block teeth of the CTD robot are analyzed in the axial direction. The interaction mechanism under reverse torque conditions reveals the tooth profile parameters and the design principle of the borehole and friction block teeth that can withstand the reverse torque while being stressed.A single-tooth simulation experiment and a single-spindle torsion coupling experiment were carried out to test the indentation and damage effects of the single tooth with different tooth shapes and different included angles on the borehole wall. The contact performance was analyzed to guide the friction block tooth design.

2. Statics Model of Friction Block Teeth of CTD Robot

During the actual drilling process, the power drill tool provides the torque to drive the drill bit to break the rock. When the drill bit breaks the rock, the rock will generate a reaction torque on the drill bit. The reaction torque is transmitted to the coiled tubing through the bottom drill tool, as shown in Figure 1. The drill bit in real drilling will produce torsional vibration, which will cause torsional vibration of the coiled tubing. Torsional vibration will reduce the sealing performance of the CTD and shorten the service life of the CTD robot. Therefore, the CTD robot developed in this paper needs to overcome the anti-torque. The CTD robot mainly overcomes the reaction torque through the contact between the friction block and the well wall.

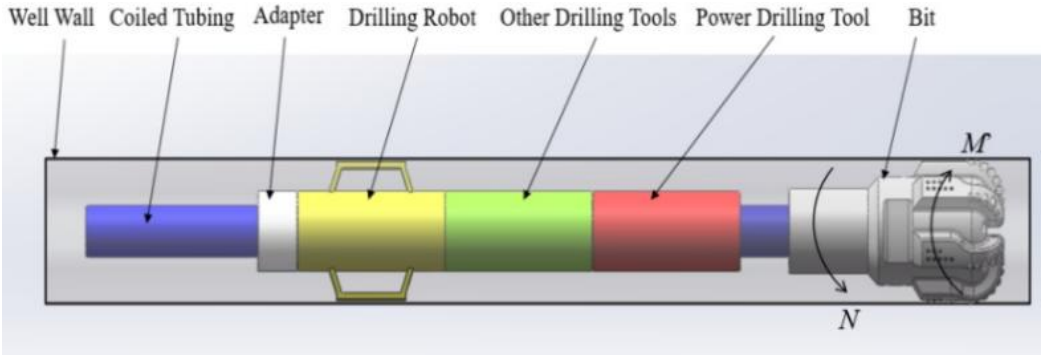

Figure 1. Schematic picture of CTD robot bearing anti-torque.

Assuming that the CTD robot has three axisymmetrically arranged support arms, there are three axisymmetrically arranged friction blocks in contact with the borehole wall. Therefore, the CTD robot shown in Figure 1 generates continuous reaction torque during the drilling process. The arrangement of the friction block teeth on the well wall is shown in Figure 2, where γ is the angle between the connecting rod and the radial direction of the drilling robot body, °, and α and β are the angle between the friction block and the push block, °.

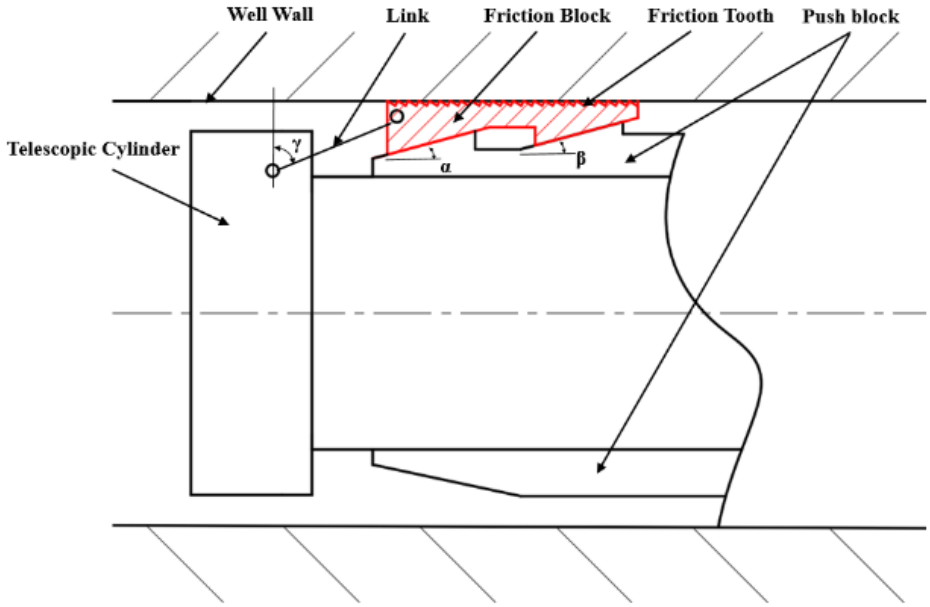

Figure 2. Schematic diagram of friction block teeth layout.

Figure 3 shows the force model of robot friction block. From the figure, it can be seen that in order to overcome the reaction torque, the CTD robot is subjected to the circumference of the well wall. The frictional force F_{fci} directly acts on the friction block of the CTD robot. The friction block of the CTD robot is also subjected to the axial friction force F_{fai} . The axial friction force is mainly to overcome the reaction force of the traction force F_T of the CTD robot.

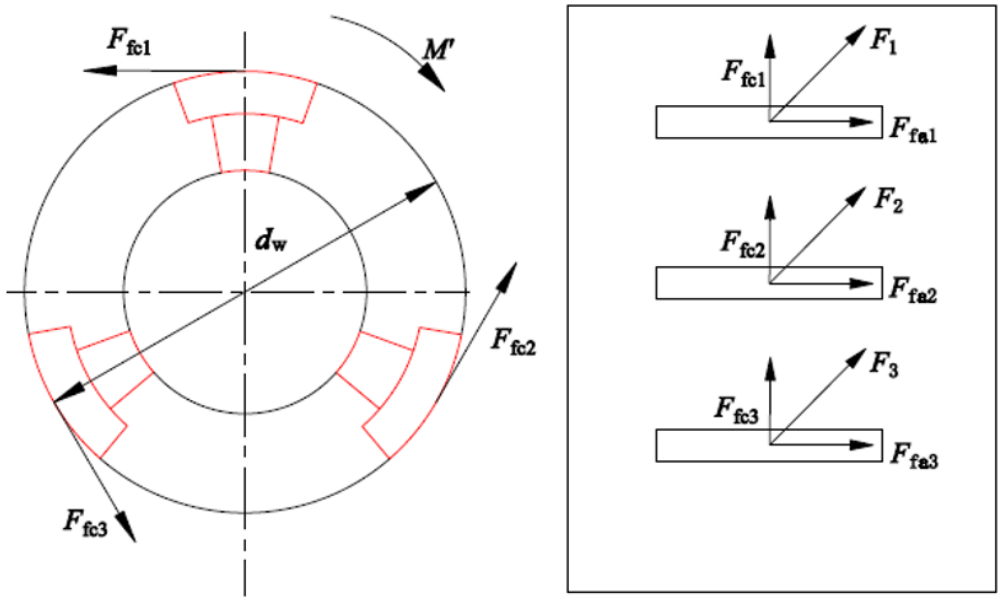

Figure 3. Analysis picture of friction block subjected to reverse torque force.

If the friction block can overcome the reaction torque generated by the rock breaking of the drill bit without slipping, the force condition in the above figure should meet the following formula:

$$\frac{d_w}{2}(F_{fc1} + F_{fc2} + F_{fc3}) = M' \tag{1}$$

where F_{fci} is the i-th circumferential friction force of the wellbore to the friction block, N; d_w is the wellbore diameter, m; and $M^{'}$ is the drill bit reverse torque, N·m.

Assuming that the circumferential friction force of the wellbore against each support block is the same, the calculation formula (2) for the circumferential friction force of any friction block can be obtained:

$$F_{fc} = \frac{2}{3}\frac{M^{'}}{d_w} \tag{2}$$

where F_{fc} is the circumferential friction force of the shaft against any friction block, N.

Considering the three friction blocks as a whole, according to the static balance relationship, the formula of axial friction and traction in Figure 3 is as follows:

$$F_{fa1} + F_{fa2} + F_{fa3} = F_T \tag{3}$$

where F_{fai} is the i-th axial friction force of the shaft against the friction block, N.

Assuming that the axial friction force of the wellbore to each support block is the same, the calculation formula for the axial friction force of any friction block can be obtained:

$$F_{fa} = \frac{1}{3}F_T \tag{4}$$

where F_{fa} is the axial friction force of the shaft against any friction block, N.

In order to increase the friction between the friction block of the CTD robot and the wellbore so that the friction block can effectively support the wellbore, teeth are usually machined on the friction block, and the teeth of the friction block are distributed at 90° to the axis of the wellbore (Figure 4).

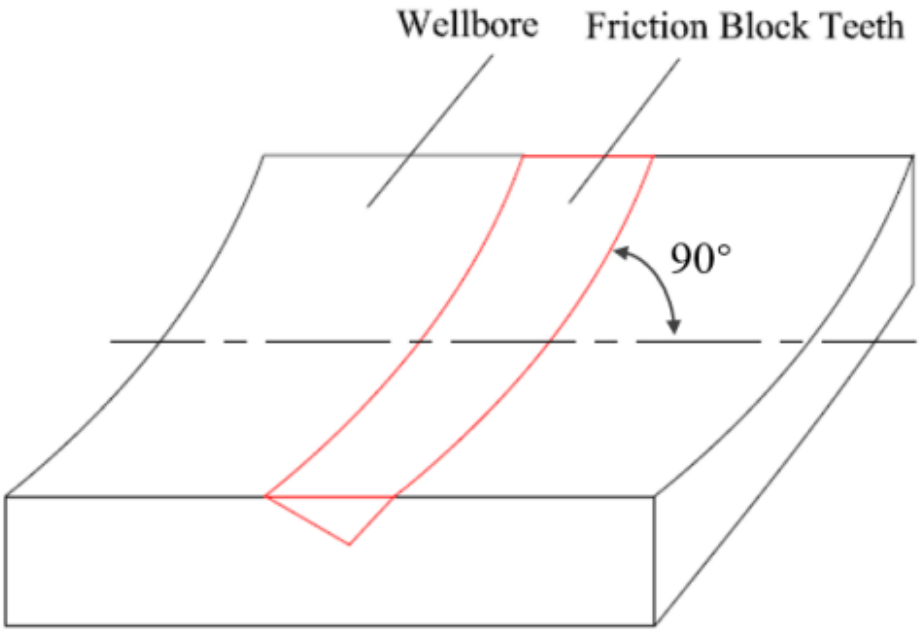

Figure 4. Schematic diagram of the contact between the friction block teeth of the CTD robot and the wellbore.

According to the working mechanism of the CTD robot, a schematic diagram of the force on a single tooth of the friction block tooth is established as shown in Figure 5.

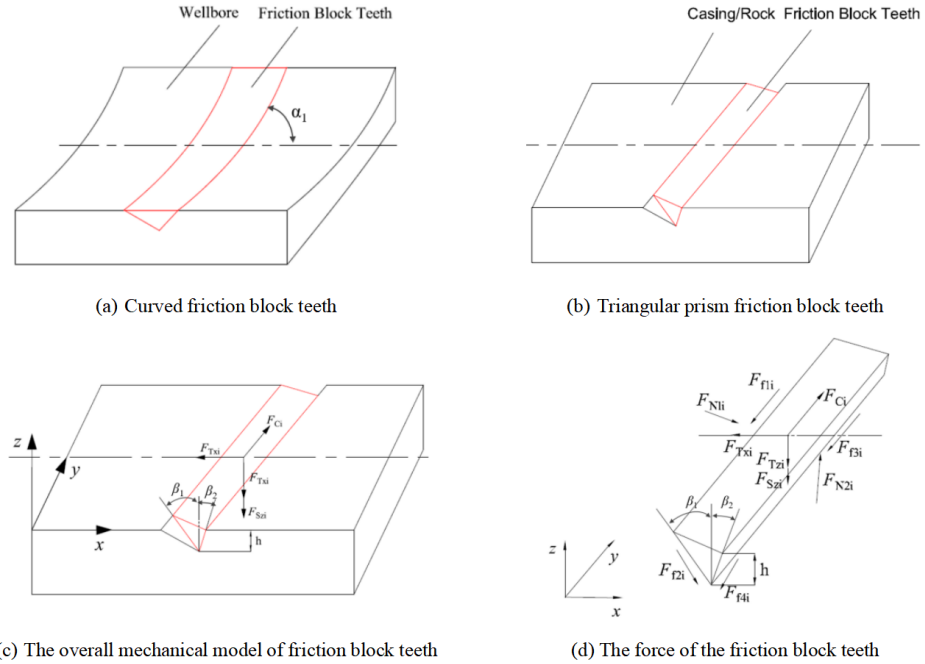

(a) Curved friction block teeth (b) Triangular prism friction block teeth

(c) The overall mechanical model of friction block teeth (d) The force of the friction block teeth

Figure 5. Schematic diagram of friction block tooth force on CTD robot friction block.

In order to simplify the calculation, the friction block teeth of the CTD robot in Figure 5a are simplified to the triangular prism friction block teeth in Figure 5b. Assuming that the teeth are grasped stably and no slippage occurs, the teeth of the friction block in Figure 5 should meet the following conditions:

$$\begin{cases} \sum F_x = 0 \\ \sum F_y = 0 \\ \sum F_z = 0 \end{cases} \tag{5}$$

From the above formula, combined with the force analysis in d, the formula is derived as follows:

$$\begin{cases} -F_{\mathrm{Txi}} - F_{\mathrm{f1i}} \cos\alpha_1 + F_{\mathrm{f2i}} \sin\beta_1 \sin\alpha_1 - F_{\mathrm{f3i}} \cos\alpha_1 + F_{\mathrm{f4i}} \sin\beta_2 \sin\alpha_1 \\ +F_{\mathrm{N1i}} \cos\beta_1 \sin\alpha_1 - F_{\mathrm{N12}} \cos\beta_2 \sin\alpha_1 = 0 \\ F_{\mathrm{ci}} - F_{\mathrm{f1i}} \sin\alpha_1 - F_{\mathrm{f2i}} \sin\beta_1 \cos\alpha_1 - F_{\mathrm{f3i}} \sin\alpha_1 + F_{\mathrm{f4i}} \sin\beta_2 \cos\alpha_1 \\ -F_{\mathrm{N1i}} \cos\beta_1 \cos\alpha_1 + F_{\mathrm{N12}} \cos\beta_2 \cos\alpha_1 = 0 \\ -F_{\mathrm{Tzi}} - F_{\mathrm{Szi}} + F_{\mathrm{N1i}} \sin\beta_1 + F_{\mathrm{N12}} \sin\beta_2 - F_{\mathrm{f2j}} \cos\beta_1 - F_{\mathrm{f4i}} \cos\beta_2 = 0 \end{cases} \tag{6}$$

where F_{Tj} is the axial traction reaction force on a single tooth of the friction block of the CTD robot, N; F_{f1i} , F_{f2i}, F_{f3i}, F_{f4i} are the friction force in different directions on a single tooth of the friction block of the CTD robot, N; α_1 is the axial-included angle of the friction block teeth of the CTD robot, °; β_1, β_2 are the tilt angle of the friction block teeth of the CTD robot, °; $F_{\mathrm{N1}i}$, F_{N2i} are the positive pressure on the inclined surface of the friction block of the CTD robot, N; F_{Ci} is the circumferential force on a single tooth of the friction block of the CTD robot, N; F_{Ni} is the radial support force of a single tooth of the friction block of the CTD robot, N.

When the friction block teeth are pressed into the casing or well wall, both sides of the teeth are subjected to the force of the casing or well wall. However, when the CTD robot is drilling normally, the front of the friction block teeth will bear the entire load, so the formula (7) can be simplified:

$$\begin{cases} F_{\mathrm{ci}} - F_{\mathrm{f1i}} \sin\alpha_1 - F_{\mathrm{N1i}} \cos\alpha_1 \cos\beta_1 = 0 \\ -F_{\mathrm{Tzi}} - F_{\mathrm{Szi}} + F_{\mathrm{N1}i} \sin\beta_1 = 0 \end{cases} \tag{7}$$

In fact, F_{f1i} and F_{N1i} should meet the following conditions:

$$F_{f1i} = \mu_1 F_{N1i} \tag{8}$$

where μ_1 is the friction coefficient between the teeth of the friction block of the robot and the wellbore constant. Combining formulas (8) and (9), the following formula can be obtained:

$$F_{Szi} = \frac{F_{ci} \sin \beta_1}{\mu_1 \sin \alpha_1 + \cos \alpha_1 \cos \beta} - F_{Tzi} \tag{9}$$

The tooth load of the friction block of the CTD robot can be obtained by the following formula:

$$\begin{cases} F_{Tzi} = \frac{F_T \cot(\alpha + \arctan \mu_2)}{3n_{teeth}} \\ F_{Szi} = \frac{F_S[\cot \gamma + \cot(\alpha + \arctan \mu_2)]}{3n_{teeth}} \\ F_{Ci} = \frac{2M'}{3d_w n_{teeth}} \end{cases} \tag{10}$$

where n_{teeth} is the number of friction teeth of the CTD robot, and d_w is the inner diameter of the wellbore, m. Combining formulas (9) and (10), the following formula can be obtained:

$$F_S = \frac{2M' \sin \beta_1}{d_w(\mu_1 \sin \alpha_1 + \cos \alpha_1 \cos \beta_1)[\cot \gamma + \cot(\alpha + \arctan \mu_2)]} - \frac{F_T \cot(\alpha + \arctan \mu_2)}{\cot \gamma + \cot(\alpha + \arctan \mu_2)} \tag{11}$$

$$F_{N1i} = \frac{F_T \cot(\alpha + \arctan \mu_2) + F_S[\cot \gamma + \cot(\alpha + \arctan \mu_2)]}{3n_{teeth} \sin \beta_1} \tag{12}$$

$$F_1 = \sqrt{F_{N1i}^2 + (\mu_1 F_{N1i})^2} = \sqrt{1 + \mu_1^2} F_{N1i} = \sqrt{1 + \mu_1^2} \frac{F_T \cot(\alpha + \arctan \mu_2) + F_S[\cot \gamma + \cot(\alpha + \arctan \mu_2)]}{3n_{teeth} \sin \beta_1} \tag{13}$$

where F_1 is the resultant force of the tooth slope of the friction block of the CTD robot, N.

3. Analysis of Influencing Factors on Statics Characteristics of Friction Block Teeth of CTD Robot

In order to analyze the static characteristics of the friction block teeth of the CTD robot, the following two points are explained for the initial parameter setting:

(1) The traction force FT of the CTD robot adopts 30,000 N;

(2) The reaction torque of the CTD robot is determined by the downhole power drilling tool screw. The downhole power drilling tool used in CTD is usually a small size power drilling tool (0.089 mm or 0.095 mm screw drilling tool). The rated torque of small screw drilling tool is about 1000 N·m, and the torque that can be provided generally does not exceed 2000 N·m, so the reaction torque it can generate will not exceed 2000 N·m. That is to say that as long as the CTD robot support mechanism can withstand sufficient reverse torque, the CTD robot can successfully drive the downhole drilling tool well. To improve the ability of the CTD robot to withstand the reverse torque, this article assumes that for the CTD robot, the maximum torque that can be withstood is 2000 N·m, that is, the reaction torque M = 2000 N·m.

(3) The number of teeth in the friction block is mainly determined by the shape of the teeth and the damage to the wellbore. In order to be able to calculate the formula (9) numerically, the number of teeth is tentatively set here as $n_{teeth} = 40$, and the inner diameter of the wellbore $d_w = 0.12$ m. $F_T = 30000$ N, $\mu 1 = 0.3, \mu 2 = 0.3$, $\beta = 15°$, $\gamma_1 = 80°$, $\eta_{teeth} = 40$, $d_w = 0.12$ m. Bring the above parameters into the formulas (11) and (13), and calculate the changes in the mechanical characteristics of the friction block teeth of the CTD robot as shown in Figures 6 and 7.

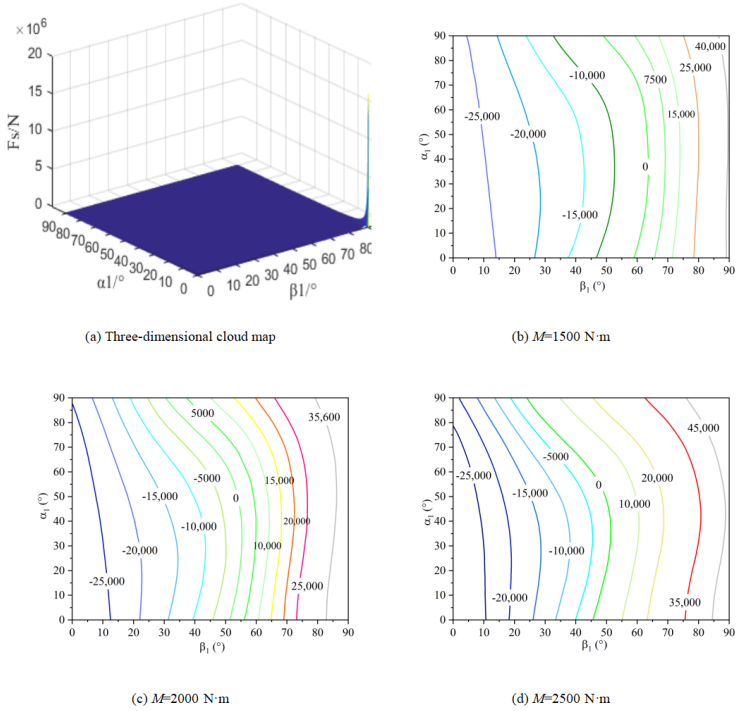

Figure 6. The law of influence of α_1, β_1, and M on supporting force.

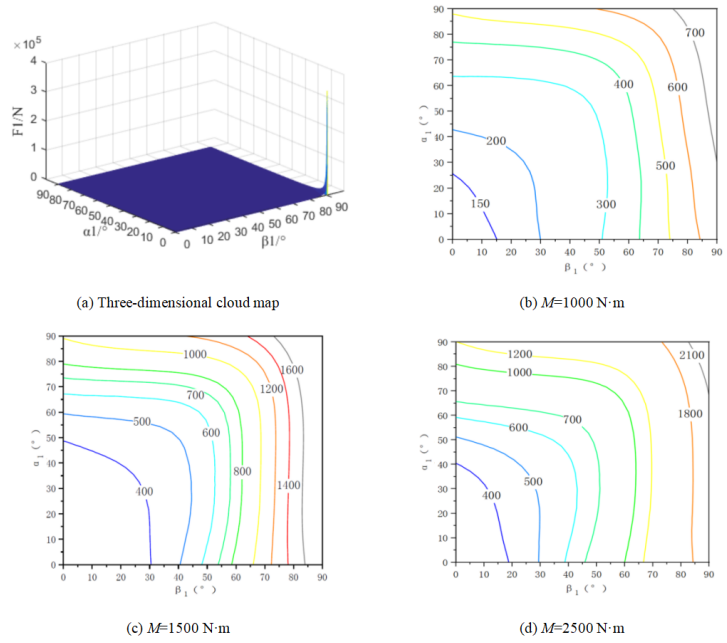

Figure 7. The law of the influence of α_1, β_1, and M on the force of teeth.

3.1. The Influence of α_1, β_1 and M on Supporting Force F_S

The following can be seen from Figure 6:

(1) With the increase in α_1, the supporting force F_S of the CTD robot increases. When β_1 is small, the change of F_S is small, and when β_1 is large, the change of F_S is large.

(2) When α_1 is a certain value, with the increase in β_1, F_S increases, and the magnitude of the change is relatively large.

(3) The curve of $F_s = 0$ is the criticality of self-locking, that is, the parameters of α_1 and β_1 are on the left side of $F_s = 0$. The friction block of the CTD robot can realize self-locking support. On the contrary, the parameters of α_1 and β_1 are at $F_S = 0$. The right side is non-self-locking support.

(4) Within the range of $a_1 < 5°$ and $\beta 1 > 85°$, the F s changes greatly, which exceeds the limit of the supporting force that the coiled tubing CTD robot can provide.

(5) As the reaction torque M increases, the self-locking critical line $F_S = 0$ shifts to the left, that is, with the increase in M , if the CTD robot is to realize the self-locking function, the β_1 angle should decrease accordingly.

3.2. The Influence of α_1, β_1 and M on the Force F_1 of Friction Block Teeth

It can be seen from Figure 7:

(1) With the increase in α_1, the force F_1 of the wellbore on the friction block teeth of the CTD robot first decreases and then increases. The reasons are as follows: (a) When the value of α_1 is relatively small, the friction block teeth can effectively resist the reaction torque. At this time, the main factor that affects F_1 is the axial force. When α_1 increases, it can be done without adding additional force, bearing part of the axial force, so F_1 is reduced. (b) When the value of α_1 is relatively large, also due to the principle of self-locking of the inclined surface, the friction block teeth can effectively resist the axial force. At this time, the main factor affecting F_1 is the reaction torque. When α_1 increases, in order to resist the action of the reaction torque, F_1 increases.

(2) As β_1 increases, F_1 increases. It can be obtained from Figure 7 that the smaller α_1 and β_1 are, the smaller F_1 is, that is, the force between the teeth and the wellbore is also smaller.

(3) As the reaction torque M increases, under the same conditions of α_1 and β_1 , F_1 increases.

3.3. The Influence of α_1,β_1 and F_T on Supporting Force F_S

Assuming M = 2000 N·m, the supporting force change law shown in Figure 8 is obtained. It can be seen from the figure that with the increase in F_T, the self-locking critical line F_S = 0 of the CTD robot shifts to the right, that is, with the increase in F_T, the optional range of β_1 is actually expanded. The reason is that the friction block is traction in the axial direction. Self-locking support can be realized in the F_T direction, and the traction force promotes the positive pressure of the friction block on the wellbore, which is much larger than the critical value of the axial slip of the friction block. The margin can offset the positive pressure of the circumferential torsion, which is much larger than the critical value of the axial slip of the friction block. The value margin can offset the positive pressure of the circumferential torsion, which is much larger than the critical value of the axial slip of the friction block, and the margin can offset the circumferential torque M. Therefore, when M does not change, the self-locking range of β_1 is expanded.

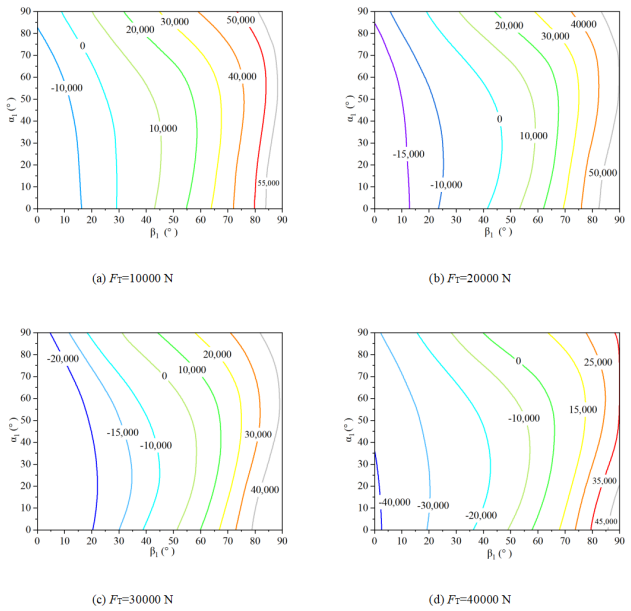

Figure 8. The influence law of α_1, β_1 F_T on supporting force F_S.

3.4. The Influence of Friction Coefficient μ_1 and μ_2 on Supporting Force F_S and F_1

Assuming F_T = 30,000 N, M = 2000 N·m, the influence law of friction coefficient on supporting force F_S as shown in Figure 9 is obtained. It can be seen from Figure 9a that (1) as μ_1 increases, F_S gradually decreases, and (2) as μ_2 increases, F_S gradually increases.

It can be seen from Figure 8b that (1) with the increase in μ_1 , F_1 gradually decreases, and (2) with the increase in μ_2 , F_1 does not change. Through the above analysis, the size of μ_1 affects $F_S$and F_1 at the same time, and the trend is opposite, so a more appropriate friction coefficient should be selected in the actual application process; μ_2 only affects F_S, but has no effect on F_1, so μ_2 should be as small as possible.

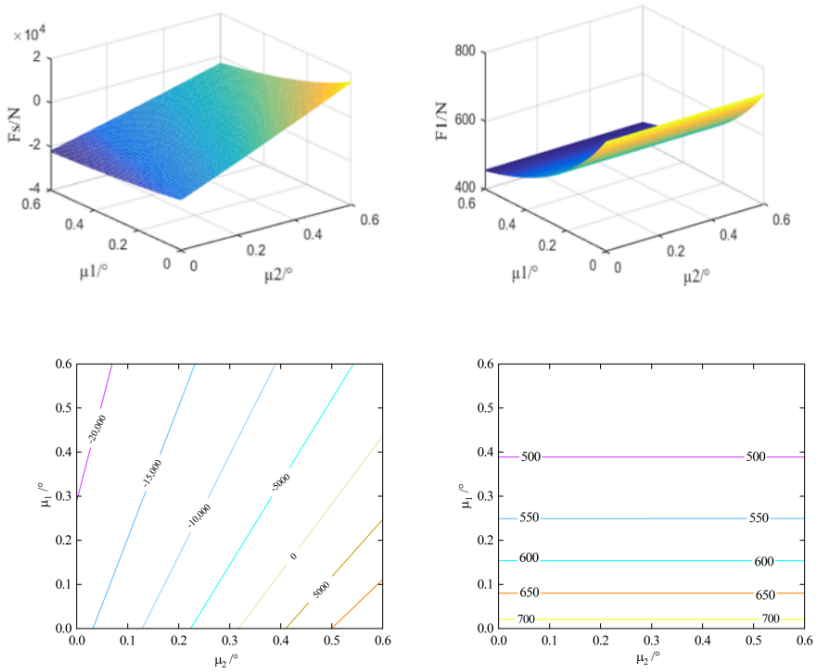

(a) The influence of friction coefficient μ_1 and μ_2 on supporting force F_S

(b) The influence of friction coefficient μ_1 and μ_2 on supporting force F_1

Figure 9. The influence of friction coefficient μ_1 and μ_2 on supporting force F_S and F_1.

3.5. The Influence of β_1, γ and M *on Supporting Force F_S*

Assuming: F_T = 30,000 N,α_1 = 45°, β_1 = 45°, the influence law of β, γ , M on supporting force on supporting force F_S as shown in Figure 9 is obtained. The following can be seen from Figure 10:

(1) With the increase in β and γ , F_S gradually increases;

(2) The self-locking critical line F_S = 0 is only related to α, and has nothing to do with γ;

(3) With the increase in M, the self-locking critical line F_S=0 moves to the left. The reason is that the friction block can achieve self-locking support in the direction of the shaft traction force F_T. The traction force promotes the positive pressure of the friction block on the wellbore. The pressure is far greater than the critical value of the axial slip of the friction block, and the positive pressure margin can offset the circumferential torque M. Therefore, when M changes, the self-locking positive pressure margin is not enough to resist the action of the torque. Therefore, in order to achieve self-locking under different torque conditions, the value of β should be calculated under the limit torque conditions.

The mechanics models developed in this paper are all based on the self-locking mechanics model. However, under complex downhole drilling conditions, if the downhole tools are prone to failure and self-locking, it may cause serious downhole sticking accidents. Therefore, the downhole tool design is being carried out. At the time, the non-self-locking structure parameters close to the self-locking condition can be selected. This solution can

not only effectively improve the working performance of the CTD robot, but also ensure that the CTD robot will not self-lock in actual working conditions.

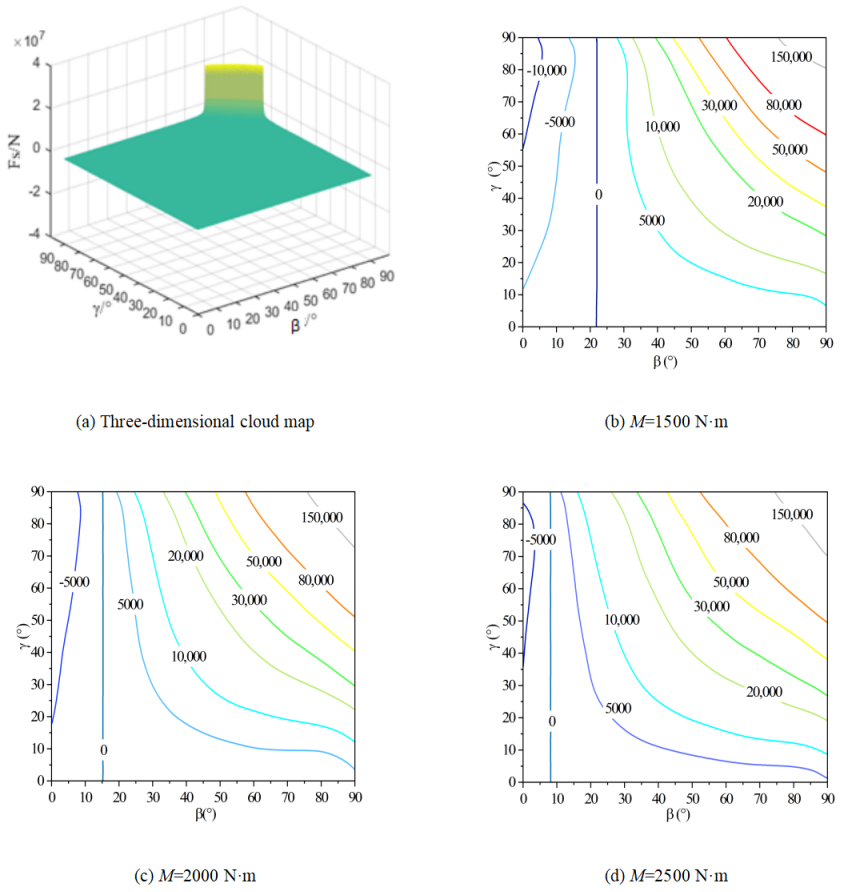

(a) Three-dimensional cloud map

(b) M=1500 N·m

(c) M=2000 N·m

(d) M=2500 N·m

Figure 10. The influence law of β, γ, M on supporting force F_S.

4. Experimental Analysis

The schematic diagram of friction block performance experiment system as shown in Figure 11. The part of the physical map of the experimental device as shown in Figure 12. The external image of experimental device as shown in Figure 13. The internal diagram of the experimental device as shown in Figure 14. The experimental goal and experimental principle are as follows:

(a) Experimental goal: By applying simulated radial positive pressure and axial traction to a single tooth, the state and performance of different single tooth profiles are tested, and the equivalent friction coefficient of the corresponding conditions is obtained. Then, the self-locking performance of different tooth profiles is judged.

By applying simulated radial positive pressure, axial traction force and lateral torque force to a single tooth, test the pressing and damage of a single tooth to the borehole wall, subject a single tooth with different angles to axial traction and lateral torque at the same time performance under the condition of force, analyze the contact effect, and obtain the equivalent friction coefficient of the corresponding condition.

(b) Experimental principle: The experiment scheme of friction block tooth single tooth is shown in the figure, in which the driving force of the hydraulic piston simulates the supporting force, axial force and torque. Install tension and compression sensors on the hydraulic piston to test the supporting force, axial force and torque, respectively. Perform rock simulation of open hole wall.

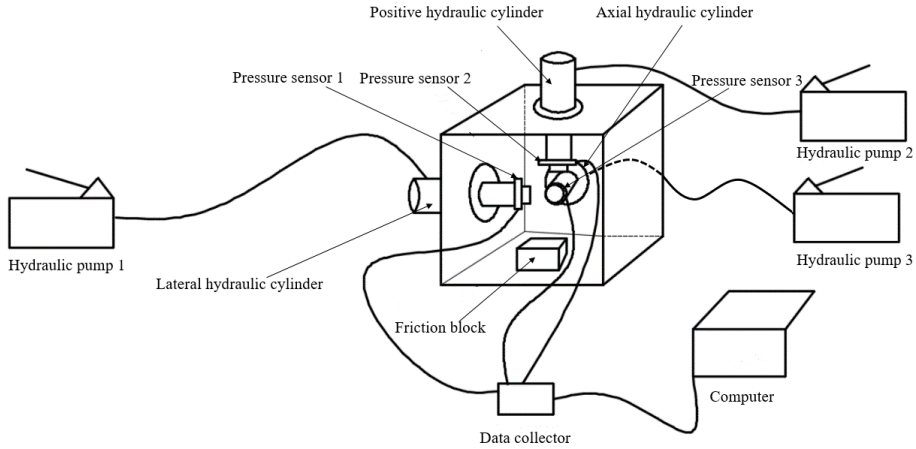

Figure 11. Schematic diagram of friction block performance experiment system.

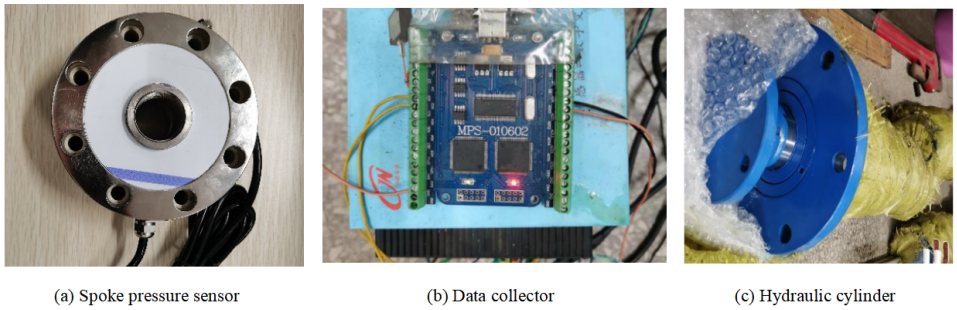

(a) Spoke pressure sensor (b) Data collector (c) Hydraulic cylinder

(d) Hydraulic pump

Figure 12. Part of the physical map of the experimental device.

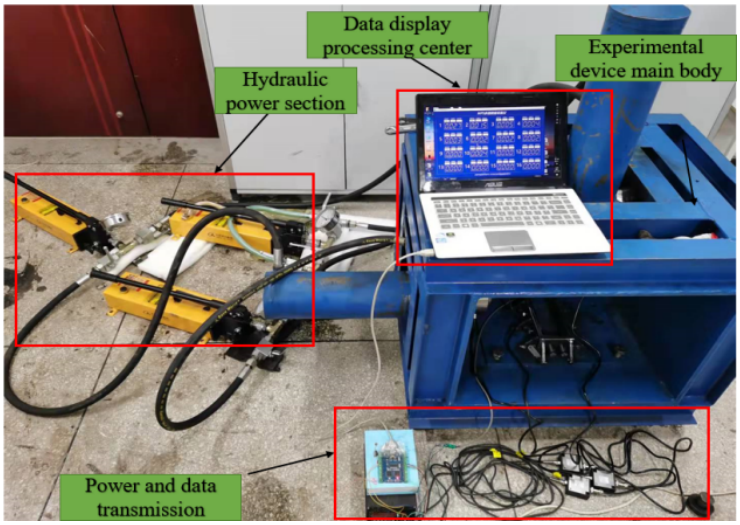

Figure 13. External image of experimental device.

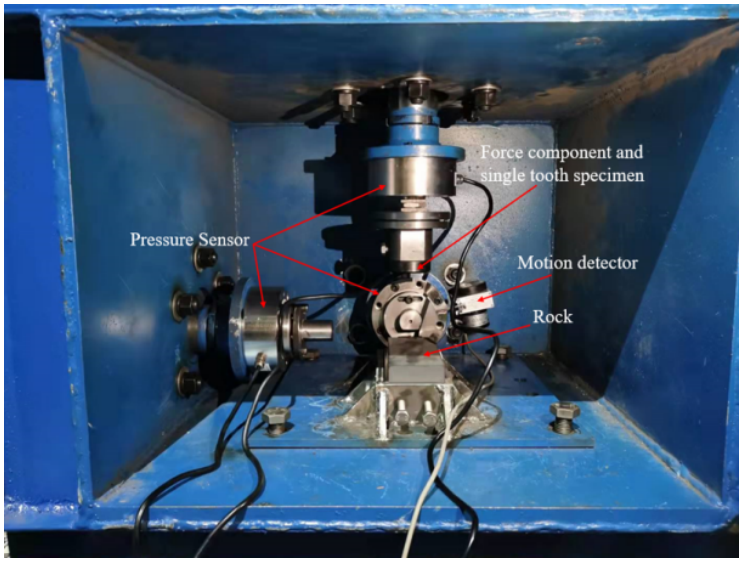

Figure 14. Internal diagram of the experimental device.

4.1. Single Tooth Simulation Experiment

Select the angle of the tilt angle of friction block teeth β_1 to be 22°–55°, and set the positive pressure range to 2000–6000 N. The single tooth specimen after quenching as shown in Figure 15. Install rock and fixed single tooth, press the forward hydraulic pump to the specified positive pressure F_N, pressurize the axial hydraulic pump, and observe the displacement. When the displacement sensor reaches 5 mm, it is regarded as the grip failure. Record the display of the axial pressure sensor at this time data F_T, and draw a data graph.

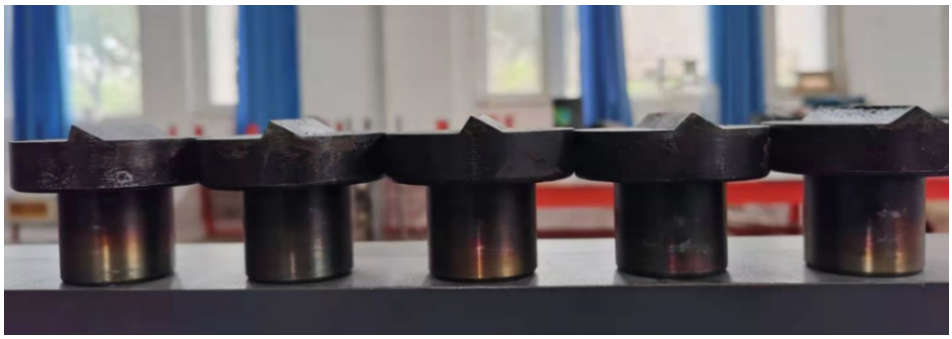

Figure 15. Single tooth specimen after quenching.

As shown in Figure 16a, the red curve in the figure is the displacement curve. One end of the displacement sensor is fixed to the inner wall of the device, and one end is fixed to the flange of the axial hydraulic cylinder, so there is an initial displacement in the figure; it starts when the friction tooth has not touched the rock sample. Record the data. After about 10s, the friction tooth touches the rock sample, and the pressure rises rapidly, reaching the set value of 2000 N in about 25 s. Starting from about 30 s, the axial hydraulic cylinder moves, and the rear force component gradually approaches the single-tooth indenter. The displacement increases rapidly; at about 40 s, the rear force application component contacts the single-tooth indenter and starts to push the single-tooth indenter to move. At this time, the axial pressure sensor display increases rapidly, and the displacement also increases slowly. During the sliding process, due to the short sliding distance, the positive pressure does not change much, and the axial force tends to be stable.

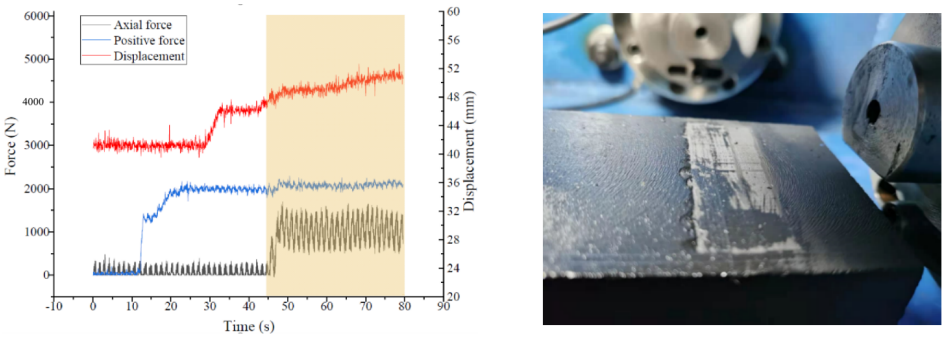

(a) Time-varying graph of simulated traction experiment parameters

(b) Experimental scratching

Figure 16. Experimental results and experimental scratching.

After intercepting the pressure data of the displacement section (shaded area of Figure 16a) and calculating the equivalent friction coefficient, the data are numerically fitted, and the friction coefficient of the stationary section is intercepted to obtain the equivalent friction coefficient as shown in Figure 17.

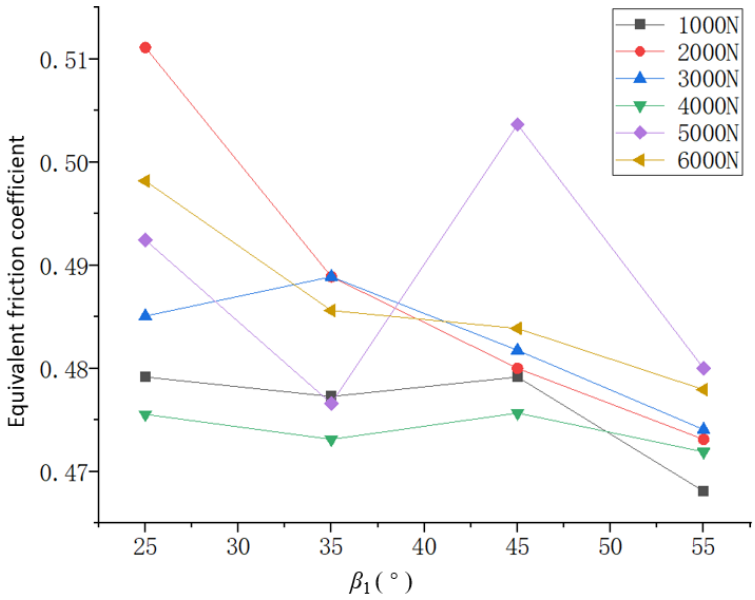

Figure 17. Comparison of experimental and numerical results

It can be seen from Figure 17 that as β_1 increases, the equivalent friction coefficient tends to gradually decrease. This is because under the same positive pressure, the increase in the rake angle leads to a decrease in the embedding depth. The sliding equivalent friction coefficient range of friction tooth contact with well wall is about 0.47–0.52. Comparing the friction coefficient of shale slab [19], it shows that setting β_1 30° on the friction block can significantly increase the equivalent friction coefficient, thereby improving the self-locking effect of the support mechanism.

4.2. Single Tooth Shaft and Torsion Coupling Simulation Contact Experiment

Select the friction teeth with the tilt angle of friction block teeth β_1 of 30°, set the positive pressure to 3000 N, respectively carry out the axial included angle of friction block teeth α_1 in the range of 60°–90°, install the rock and the fixed single tooth, and pressurize the positive hydraulic pump to the specified positive force F_N. The axial hydraulic pump and lateral hydraulic pump apply pressure at the same time. When there is obvious sliding,

record the data displayed by the pressure sensor at this time axial force F_T and lateral force F_{Tm}, and draw the data graph.

The curve changes of the axial force and the lateral force in Figure 18 are almost synchronized, which realizes the design and simulation of the shaft torsion coupling load, and the effect of simultaneous loading of the axial force and the lateral force. Due to the load in both directions at the same time, due to the sensor error, the lateral force output load fluctuation in the figure is relatively large, but the values and laws of the two are almost the same, so the two calculations are based on the same equivalent friction coefficient.

Summarize the values obtained from the fitting curve in the figure, calculate the equivalent friction coefficient, and establish the same multi-directional force numerical model of the helical tooth in the simulation software to obtain the simulated axial and lateral equivalent friction coefficients of the numerical calculation. Draw them together as shown in Figure 19.

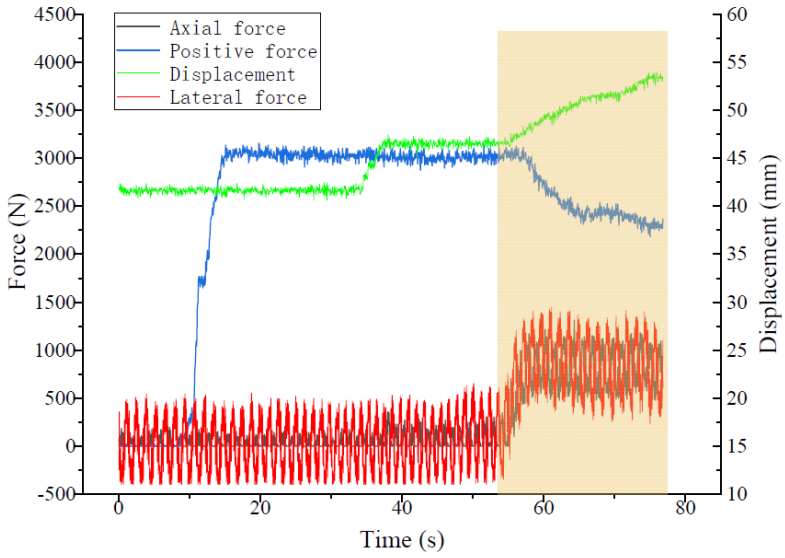

Figure 18. Time−varying graph of simulated shaft and torsion coupling experiment parameters.

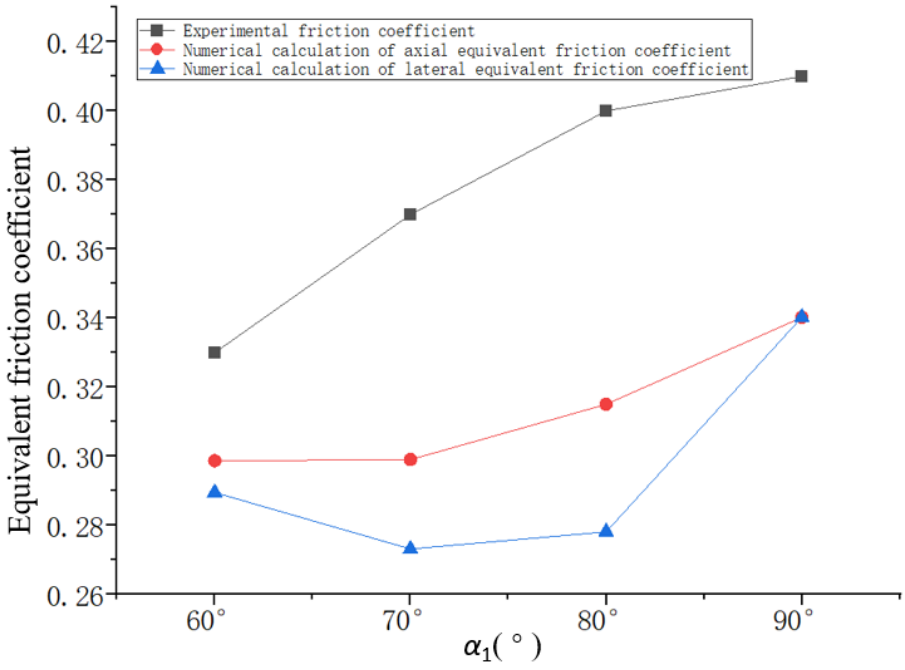

Figure 19. Comparison of experimental and numerical results.

It can be seen from Figure 19 that the equivalent friction coefficient obtained under the single-tooth simulation shaft and torsion coupling condition is slightly smaller than the value obtained in the experiment compared with the friction coefficient of the numerical simulation. Therefore, under the condition of similar friction coefficients between materials, the slaw of numerical simulation and experiment are similar, and both show a downward trend, but the value of the equivalent friction coefficient is low, indicating that the actual sliding load of the tooth is not deep in the actual contact. It should be greater than the result of the numerical simulation. When the experimental equivalent friction coefficient is 0.33–0.41, and α_1 is about 90°, the self-locking performance is the best.

5. Discussion

The coiled tubing drilling technology with low cost and low pollution has been widely used, but the "buckling locking" problem of coiled tubing in long horizontal wells restricts the promotion of this technology. The use of drilling robot traction is the main means to solve these problems. The research found that the friction teeth in the support mechanism of the drilling robot have a great impact on its support performance. At present, the research on the mechanical properties of the downhole drilling robot is mainly focused on the mechanical properties of its support mechanism, and the research on the mechanical properties of the friction block teeth of the drilling robot has not been carried out. In this paper, a static model of the friction block teeth of the coiled tubing drilling robot under the conditions of axial traction and reverse torque is established. The friction block teeth of the CTD robot are analyzed in the axial direction. In the future work, the mechanical properties of the support mechanism are combined with the static characteristic of the friction block teeth to research the performance of the coiled tubing drilling robot.

6. Conclusions

According to the requirements of the CTD robot's large traction force and small size, this paper mainly carried out the research on the statics characteristics of the friction block of the CTD robot's large traction force support mechanism.

(1) Based on the research of domestic and foreign literature, analyzing the mechanical characteristics of the supporting mechanism of the drilling robot, combined with the actual working conditions of CTD, a static model of the friction block teeth of the CTD robot under the combined action of anti-torque and axial load is established. When teeth are processed on the friction block, the critical condition for autonomous support of the inclined block will change, that is, the inclination angle of the support block that plays a role in self-locking will increase. The axial included angle of the friction block teeth is $\alpha_1 > 5°$, and the inclination angle of the friction block teeth is $\beta_1 < 85°$, which can effectively assist self-locking. The CTD robot bears the axial load and the torsional load at the same time. When the torsional load is smaller than the axial load to a certain extent, the CTD robot can realize self-locking support. This is because the axial load is torsion while achieving axial self-locking. The load provides a certain amount of axial self-locking support force margin.

(2) Through analysis, it is found that the CTD robot can only be locked under the reaction torque, that is, use the support force margin generated by the axial traction force to withstand the reaction torque of the CTD robot. When the reaction torque of the drilling robot is greater than the traction force, the support of the CTD robot will fail with the generated supporting force margin, so the CTD robot cannot achieve anti-torque self-locking.

(3) The interaction mechanism between different tooth parameters and the well wall/pipe wall is revealed, and the design principle of friction block teeth that can withstand the reaction torque while providing axial force is obtained.

(4) Through a single-tooth simulation traction experiment, under the condition of a positive pressure of 1000-6000 N and the tilt angle of friction block teeth β_1 25–55°, the equivalent friction coefficient calculated by the experiment is in the range of 0.47–0.51. Through the single pinion torsion coupling simulation contact experiment, when β_1 is 30°,

the positive pressure is 3000 N, the axial included angle of the friction block teeth α_1 is 60–90°, and the equivalent friction coefficient calculated by the experiment is in the range of 0.33–0.41. Combining the two, it is obtained that the self-locking performance is the best when β_1 is about 30° and α_1 is about 90°. This provides a reference for the design of the friction teeth of the support mechanism.

Author Contributions: J.Z., methodology, writing—original draft, funding acquisition; S.H., conceptualization, methodology, writing—original draft; X.X., writing—review and editing, data curation; X.Z., writing—review and editing, investigation; R.Y., supervision. All authors have read and agreed to the published version of the manuscript.

Funding: National Natural Science Foundation of China (No. 52004232, U19A200380), Sichuan Science and Technology Program (2023YFQ0061, 2022YFQ0061, JG2021-624).

Institutional Review Board Statement: Not applicable.

Informed Consent Statement: Not applicable.

Data Availability Statement: There are no associated data in this study.

Acknowledgments: This work was supported by China Petroleum Group Chuanqing Exploratory Drilling Engineering Co., Ltd. We thank China Petroleum Group Chuanqing Exploratory Drilling Engineering Co., Ltd. for providing suggestion.

Conflicts of Interest: The authors declare no conflict of interest.

Abbreviations

The following abbreviations are used in this manuscript:

CTD Coiled tubing drilling

References

1. Li, H.; Huang, B.S.; Liu, Q.Y. Micro-borehole drilling technology and its application prospect. *Drill. Prod. Technol.* **2008**, *31*, 42–45.
2. Liu, Q.Y.; Zhai, D.; Li,W. Application of coiled tubular drilling technology in domestic unconventional gas development. *China Pet. Mach.* **2011**, *39*, 94–97.
3. Liu, Q.Y. Smart drilling system in future. *CAAI Trans. Intell. Syst.* **2009**, *4*, 16–20. [CrossRef]
4. McIntosh, T.; Baros, K. J.; Gervais, J. G.; Schultz, R.; Whitworth, J. A vibratory tool study on extended reach horizontals during coiled tubing drill out in the eagle ford shale. In Proceedings of the SPE/ICoTA Coiled Tubing and Well Intervention Conference and Exhibition, Houston, TX, USA, 22–23 March 2016.
5. He, L.; McAllister, J.; Hawkins, J.; Turner, M. Application of downhole tractor in gas well zonal isolation. In Proceedings of the SPE/ICoTA Well Intervention Conference and Exhibition, The Woodlands, TX, USA, 24–25 March 2020.
6. Livescu, S.; Craig, S. A critical review of the coiled tubing friction-reducing technologies in extended-reach wells. *J. Pet. Sci. Eng.* **2017**, *157*, 747–759. [CrossRef]
7. Baez, F.; Alali, A. Drilling performance improvements in gas shale plays using a novel drilling agitator device. In Proceedings of the 2011 AADE National Technical Conference & Exhibition, The Woodlands, TX, USA, 14–16 June 2011.
8. Yue, Q. B.; Liu, J.B.; Zhang, L.G.; Zhang, Q. The posting-buckling analysis and evaluations of limit drilling length for coiled tubing in the sidetrack horizontal well. *J. Pet. Sci. Eng.* **2018**, *164*, 559–570.
9. Jorgen, H. Radial Piston Motor or Pump. U.S. Patent 5391059, 21 February 1995.
10. Formica, J.; Wise, J.; Boye-Moller, C.; Davis, B.; Godfrey, B.; Walker, C. Tractor-conveyed sensors and chemical packer are utilized to remediate an extended-reach horizontal uncemented slotted liner completion in a siliceous shale reservoir, Kern County, California. In Proceedings of the SPE International Thermal Operations and Heavy Oil Symposium and Western Regional Meeting, Bakersfield, CA, USA, 16–18 March 2004.
11. Duthie, L.; Saiood, H.; Anizi, A.; Moore, B. First worldwide slim coiled-tubing logging tractor deployment. *SPE Prod. Oper.* **2022**, *37*, 88–98. [CrossRef]
12. Chen, L.; Gao, D.; Sun, T. Characteristics of process of surmounting obstacles by downhole tractors in horizontal shafts. *Chem. Tech. Fuels Oil.* **2017**, *5*, 569–578. [CrossRef]
13. Zhao, J.G.; Liu, Q.Y.; Zhu, H.Y.; Wang, Z.D.; Liu, W.Q. Nonlinear dynamic model and characteristization of coiled tubing drilling system based on drilling robot. *J. Vib. Eng. Technol.* **2021**, *9*, 541–561. [CrossRef]
14. Zhao, J.G.; P, H.X.; Fang, S.J.; Wang, K.P.; Han, S.; Zhang, Y.; Zhu, Z.X.; Tu, C. Study on dynamic sealing performance of combined sealing structure of telescopic type of downhole robot by using HTHP coupling method. *Proc. Inst. Mech. Eng. Part C* **2021**, *104*, 368504211013214. [CrossRef] [PubMed]

15. Zhao, J. G.; Han, S.; Liu, Q.Y.; Zhang, Y. Combined control mechanism of WOB and ROP with downhole robot in coiled tubing drilling process. *SPE J.* **2021**, *27*, 153–166. [CrossRef]
16. Wei, H.; Wu, W.; Wang, Z. Structure design of downhole robot in oil Well. *Appl. Mech. Mater.* **2011**, *80–81*, 996–999. [CrossRef]
17. Li, L.; Zhou, D.; Zhang, G.; Li, Y.; Song, W. Optimal design of horizontal well traction robot traction force regulating mechanism. *Adv. Mat. Res.* **2014**, *1033–1034*, 1350–1353. [CrossRef]
18. Qiao, J.; Shang, J.; Goldenberg, A. Development of inchworm in-pipe robot based on self-locking mechanism. *IEEE ASME Trans. Mechatron.* **2013**, *18*, 799–806. [CrossRef]
19. Zhou, J.; Jiang, T.X. Experimental study and mechanical properties analysis of fracture propagation in shale formation, Sichuan Basin. *SCPMA* **2017**, *47*, 153–160. [CrossRef]